Waveguides induced by photorefractive screening solitons

Ming-feng Shih, Zhigang Chen, Matthew Mitchell, and Mordechai Segev

Department of Electrical Engineering and Center for Photonics and Optoelectronic Materials, Princeton University, Princeton, New Jersey 08544

Howard Lee, Robert S. Feigelson,* and Jeffrey P. Wilde†

Department of Applied Physics, Stanford University, Stanford, California 94305

Received May 14, 1997

We study theoretically and experimentally the properties of waveguides induced by one-dimensional steady-state photorefractive screening solitons. We show that the number of possible guided modes in a waveguide induced by a bright soliton depends on the intensity ratio of the soliton, which is the ratio between the soliton peak intensity and the sum of the background illumination and the dark irradiance. We find that the number of guided modes increases monotonically with increasing intensity ratio. By adjusting the intensity ratio and the applied field, one can keep a fixed soliton size and at the same time vary the number of guided modes continuously. On the other hand, waveguides induced by dark screening solitons can support only one guided mode for all intensity ratios. Our experiments show good agreement with the theoretical results for both bright- and dark-soliton-induced waveguides. © 1997 Optical Society of America [S0740-3224(97)00412-8]

1. INTRODUCTION

Photorefractive spatial solitons have attracted substantial research interest since their existence was predicted[1] and observed[2] a few years ago. Three types of photorefractive bright and dark solitons have been discovered thus far, including quasi-steady-state solitons,[1,2] photovoltaic solitons,[3,4] and screening solitons.[5–8] They all rely on a change in the refractive index driven by space-charge fields (via the electro-optic effect) to balance diffraction. The quasi-steady-state solitons exist in bright[2] and dark[9] forms and in one and two transverse dimensions when an externally applied electric field is slowly being screened. Photovoltaic solitons occur in photorefractive materials with a strong photovoltaic current (e.g., $LiNbO_3$). Thus far, only dark photovoltaic solitons have been observed, including both one-[4] and two-dimensional solitons (with the latter referred to as vortex solitons[10]). Screening solitons exist in a photorefractive material when an externally applied field is nonuniformly screened at steady state. Screening solitons have been thus far reported in one-[11] and two-dimensional[7] bright and one-dimensional dark[12] realizations.

In general, the properties of photorefractive spatial solitons greatly differ from those of Kerr-type solitons in three aspects: (1) Photorefractive spatial solitons are stable when trapped in either one or two transverse dimensions. (2) The required optical power for formation of photorefractive solitons is very low (as low as 1 μW, compared with 100 kW for optical Kerr solitons). (3) Since the response of photorefractive media is wavelength dependent, one can generate a soliton with a very weak beam and guide within it a much more intense beam of a wavelength at which the material is less photosensitive.[13] This enables the steering and controlling of intense beams by use of weak (soliton) beams. Therefore photorefractive spatial solitons seem very promising for various applications, such as all-optical control of beam steering and optical wiring, near-field multichannel interconnects, and frequency conversion in soliton-induced waveguides (see discussion on potential applications in Ref. 14). Some preliminary experiments, such as soliton waveguiding[13,15] and coherent or incoherent soliton collisions of either one- or two-dimensional bright solitons, have been demonstrated very recently.[16–19] However, the theory of the core idea, that is, waveguides being induced by photorefractive solitons, has not been fully investigated yet.

In this paper, we analyze the properties of waveguides induced by one-dimensional steady-state photorefractive screening solitons. We show that the number of possible guided modes in a waveguide induced by a bright soliton depends on the intensity ratio of the soliton, which is the ratio between the soliton peak intensity and the sum of the background illumination and dark irradiance. We find that the number of guided modes increases monotonically with increasing intensity ratio starting from a single mode. When the intensity ratio is much smaller than unity (defined as the Kerr limit[14]), the waveguide can support only one mode for guided beams of wavelengths equal to or longer than that of the soliton. On the other hand, waveguides induced by dark screening solitons can support only a single guided mode for all intensity ratios. Our experiments show good agreement with the theoret-

0740-3224/97/113091-11$10.00

ical results for both bright- and dark-soliton-induced waveguides.

2. WAVEGUIDES INDUCED BY BRIGHT AND DARK SOLITONS

We follow the steps of a previous paper[14] on one-dimensional photorefractive screening solitons to derive bright and dark soliton solutions. We start from the standard set of rate and continuity equations and Gauss' law, which describes the photorefractive effect with electrons being the sole charge carriers, plus the wave equation for the slowly varying amplitude of the optical field:

$$(s|A|^2 + sI_b + \beta)(N_d - N_d^i) - \gamma \hat{n} N_d^i = 0, \tag{1}$$

$$\nabla \cdot \hat{J} = \nabla \cdot (q\mu \hat{n}\hat{E} + k_B T \mu \nabla \hat{n}) = 0, \tag{2}$$

$$\nabla \cdot \hat{E} + (q/\varepsilon_s)(\hat{n} + N_A - N_d^i) = 0, \tag{3}$$

$$\left(\frac{\partial}{\partial z} - \frac{i}{2k}\frac{\partial^2}{\partial x^2}\right) A(x, z) = \frac{ik}{n_b}\Delta n(\hat{E}) A(x, z), \tag{4}$$

$$V = -\int_{-l/2}^{l/2} \mathrm{d}x \cdot \hat{E}, \tag{5}$$

where $\Delta n(\hat{E}) = -(1/2) n_b{}^3 r_{\mathrm{eff}} \hat{E}$ is the electro-optic change in the refractive index, and the independent variables are z, the longitudinal coordinate (propagation axis), and x, the transverse coordinate. The five dependent variables are $\hat{n}$, the electron number density; N_d^i, the number density of ionized donors; $\hat{J}$, the current density; $\hat{E}$, the space-charge field inside the crystal; and A, the slowly varying amplitude of the optical field, defined by $E_{\mathrm{opt}}(x, z, t) = A(x, z)\exp(ikz - i\omega t) + \text{c.c.}$ ($k = 2\pi n_b/\lambda$, and ω is the optical frequency). Relevant constants of the crystal are N_d, the total donor number density; N_A, the number density of negatively charged acceptors that compensate for the ionized donors; β, the dark generation rate; s, the photoionization cross section; γ, the recombination rate coefficient; μ, the electron mobility; ε_s, the low-frequency dielectric constant; r_{eff}, the effective electro-optic coefficient; V, the external voltage applied to the crystal between electrodes separated by distance l; $-q$, the charge on the electron; k_B, Boltzmann's constant; and T, the absolute temperature. We also define the optical, background, and dark irradiances as $I(x) = |A(x, z)|^2$, I_b, and $I_{\mathrm{dark}} = \beta/s$, respectively. Typically, I_{dark} is very small as compared to I_b of 1 mW/cm^2 (or larger) in most photorefractive materials. We seek soliton solutions of the form

$$A(x, z) = u(x)\exp(i\Gamma z)(I_{\mathrm{dark}} + I_b)^{1/2}, \tag{6}$$

where Γ is defined as the soliton propagation constant and $u(x)$ is the normalized amplitude. We transform the equations to dimensionless form by the substitutions $n = \hat{n}/N_d$, $r = N_d/N_A$, $N = N_d^i/N_d$, $E = \hat{E}/(V/l)$, $J = |\hat{J}|/(q\mu N_d V/l)$, and $\xi = x/d$, where $d = (\pm 2kb)^{-1/2}$ is the characteristic length scale for the soliton, and $b = (k/n_b)[(1/2) n_b{}^3 r_{\mathrm{eff}} V/l] \equiv (k/n_b)\Delta n_0$ is the parameter that characterizes the strength and the sign of the optical nonlinearity [Δn_0 is the net change in the refractive index in the dark, i.e., $I(x) = 0$, for all x]. In the low-intensity regime, that is, under the condition $4ar(u^2 + 1) \ll 1/r \ll 1$,[14] where $a = s(I_{\mathrm{dark}} + I_b)/(\gamma N_d)$, the nonlinear differential equation, derived with perturbative methods for the normalized soliton amplitude, is

$$\frac{\mathrm{d}^2 u}{\mathrm{d}\xi^2} \mp \left(\frac{\eta}{u^2 + 1} - \frac{\Gamma}{b}\right) u = 0. \tag{7}$$

The upper (lower) sign represents the bright (dark) soliton with $\eta = 1$ [$\eta = (1 + u_\infty{}^2)$] and $\delta \equiv \Gamma/b = \ln(u_0{}^2 + 1)/u_0{}^2$ ($\delta \equiv \Gamma/b = 1$). The boundary conditions for a bright soliton are (i) $u(\infty) = u'(\infty) = u''(\infty) = 0$, (ii) $u'(0) = 0$, and (iii) $u''(0)/u(0) < 0$, while the boundary conditions for a dark soliton are (i) $u(\infty) = u_\infty$, (ii) $u'(\infty) = u''(\infty) = 0$, (iii) $u(0) = 0$, and (iv) a real $u'(0)$. The space-charge field,

$$E = -\eta/(u^2 + 1), \tag{8}$$

is present in the photorefractive material after the steady-state screening soliton has formed. It gives rise to a change in the refractive index, $\Delta\bar{n}(x) = \Delta n_0/(1 + u^2)$.

Consider now a probe beam propagating in this soliton-induced (graded-index) waveguide and with an optical electric field, $\bar{E}_{\mathrm{opt}}(x, z, t) = v(x)\exp(i\bar{\beta}z - i\bar{\omega}t) + \text{c.c.}$ ($\bar{\omega}$ is the frequency of the probe beam, and $\bar{\beta}$ is the propagation constant). The wave equation for the slowly varying amplitude $v(x)$ is

$$\frac{\mathrm{d}^2 v}{\mathrm{d}x^2} + [\bar{k}_0{}^2 \bar{n}^2(x) - \bar{\beta}^2] v = 0, \tag{9}$$

with the refractive index,

$$\bar{n}(x) = \bar{n}_b + \Delta\bar{n}(x) = \bar{n}_b - \frac{1}{2}\bar{n}_b{}^3 \bar{r}_{\mathrm{eff}} \hat{E}(x), \tag{10}$$

and the wave vector in vacuum, $\bar{k}_0 = 2\pi/\bar{\lambda} = \bar{\omega}/c$. The values of unperturbed refractive index $\bar{n}_b$ and the electro-optic coefficient $\bar{r}_{\mathrm{eff}}$ are now at the new frequency $\bar{\omega}$. Note that both $\bar{n}_b$ and $\bar{r}_{\mathrm{eff}}$ are polarization dependent.

A. Waveguides Induced by Bright Solitons

To generate a bright screening soliton, Δn has to be negative, as does (V/l).[14] Using the electric field that supports the solitons [from Eq. (8)] and the normalization $E = \hat{E}/(V/l)$, we obtain the refractive index

$$\bar{n}(x) = \bar{n}_b + \frac{1}{2}\bar{n}_b{}^3 \bar{r}_{\mathrm{eff}} \frac{V}{l} \frac{1}{u^2(x) + 1}. \tag{11}$$

Typically, for a spatial soliton, $|\Delta n_0/n_b| \leqslant 10^{-3}$; thus $|b/k| = |\Delta n_0/n_b| \ll 1$, and we can rewrite Eq. (9) as

$$\frac{\mathrm{d}^2 v}{\mathrm{d}\bar{\xi}^2} = -\left[\bar{\delta} - \frac{1}{u^2(\bar{\xi}/\alpha_1\alpha_2) + 1}\right] v, \tag{12}$$

where

$$\bar{\delta} = \frac{\bar{\beta}^2 - \alpha_1{}^2 k^2}{2kb\,\alpha_1{}^2 \alpha_2{}^2}, \tag{13}$$

is the normalized propagation constant, and $\bar{\xi} = \alpha_1\alpha_2\xi$ is the new normalized length with two normalization factors,

$$\alpha_1 = \frac{\bar{\lambda}}{\lambda}\frac{\bar{n}_b}{n_b}, \tag{14}$$

$$\alpha_2 = \frac{\bar{n}_b}{n_b}\sqrt{\frac{\bar{r}_{\text{eff}}}{r_{\text{eff}}}}. \tag{15}$$

Solving Eq. (12) gives the guided modes of the waveguide induced by a bright screening soliton. Notice that if $\alpha_1 = \alpha_2 = 1$, that is, if the probe beam is of the same polarization and of the same wavelength as the soliton beam, one of the eigenfunctions of Eq. (12) is identical to $u(\xi)$ with the eigenvalue $\bar{\delta} = \delta = \Gamma/b$ [or $\bar{\beta} = k + \Gamma$ since $|\Gamma| \ll k$; one can see this directly by comparing Eq. (12) with Eq. (7), when bright solitons are applied, i.e., $\eta = 1$, and the upper sign is chosen]. In other words, the soliton is a guided mode of the waveguide it induces. Since the amplitude of the bright soliton, $u(\xi)$, never crosses the zero point, the soliton is indeed the first (fundamental) guided mode of its own induced waveguide. This principle is generally true for all bright spatial solitons.[20,21]

We now wish to find the guided modes, $v(\bar{\xi})$, in a waveguide induced by the soliton $u(\xi)$. First, we solve Eq. (7) numerically for various values of u_0 and find the soliton

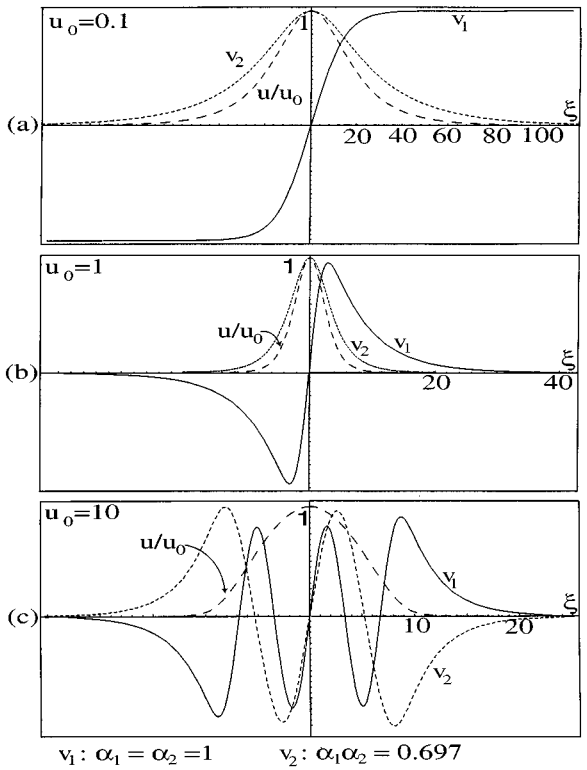

Fig. 1. Amplitude profiles of the bright screening soliton $u(\xi)$ (dashed curves) and of the highest guided mode [$v_1(\xi)$, solid curves for $\alpha_1 = \alpha_2 = 1$; $v_2(\xi)$, dotted curves for $\alpha_1\alpha_2 = 0.697$] of the soliton-induced waveguide at (a) $u_0 = 0.1$, (b) $u_0 = 1$, and (c) $u_0 = 10$. $u(\xi)$ is normalized to u_0 and $v_1(\xi)$, $v_2(\xi)$ to the maximum of $v_1(\xi)$ and $v_2(\xi)$, respectively. At $u_0 = 10$, there are six guided modes for $\alpha_1 = \alpha_2 = 1$ and four modes for $\alpha_1\alpha_2 = 0.697$.

wave forms $u(\xi)$. Several particular cases are shown by the dashed curves in Fig. 1, where we plot the normalized amplitude $u(\xi)/u(0)$. Because $u(\xi)$ does not have a closed-form solution, we use a numerical shooting method to solve Eq. (12) for $v(\bar{\xi})$ and then transfer it back to $v(\xi)$, so that both $u(\xi)$and $v(\xi)$ can be shown on the same plot. In real space, the propagation constant of a guided mode, $\bar{\beta}$, should lie between the maximum and the minimum values of the refractive index $\bar{n}(x)$ times $\bar{k}_0$ (as in any dielectric waveguide). Therefore, in Eqs. (12) and (13), the eigenvalue, $\bar{\delta}$, must be in the range between $1/(1 + u_0^2)$ and unity to obtain a bound eigenfunction $v(\bar{\xi})$. By repetitively guessing $\bar{\delta}$ in that range, integrating Eq. (12) numerically, and looking for a bound solution, $v(\pm\infty) \neq \pm\infty$, we are able to calculate all the bound eigenfunctions. Figure 1(a) shows that when $\alpha_1 = \alpha_2 = 1$ (and thus $\bar{\xi} = \xi$), the second guided mode (solid curve, v_1) of the soliton-induced waveguide at $u_0 = 0.1$ is roughly at the cutoff, i.e., $v(\xi \to \pm\infty) \neq 0$ with $v'(\xi \to \pm\infty) = v''(\xi \to \pm\infty) = 0$. We find that for all $u_0 < 0.02$ the induced waveguide is single mode for $\alpha_1 = \alpha_2 = 1$. On the other hand, for $u_0 = 1$, there are two guided modes [Fig. 1(b): the first mode coincides with $u(\xi)$, and the second, v_1, is shown by the solid curve] and for $u_0 = 10$ there are six guided modes [Fig. 1(c): only the sixth mode is shown here as the solid curve, v_1]. In Fig. 2, we show the normalized propagation constants of the guided modes as functions of u_0 in the range $0 \leq u_0 \leq 20$. The number of guided modes at each u_0 is given by the number of intersections of the dashed vertical lines with the curves of the propagation constant in Fig. 2. The three dashed lines correspond to $u_0 = 0.1$, 1, and 10 (the examples given in Fig. 1). Notice that the number of guided modes increases monotonically with increasing u_0. Similar results are obtained when the same approach is used for different values of α_1 and α_2. Figure 3 shows the number of guided modes and the propagation constants as a function of u_0 when $\alpha_1\alpha_2 = 0.697$, which corresponds to a bright soliton at a 488-nm wavelength in a SBN:60 crystal with $r_{\text{eff}} = 307$ pm/V and guided within it a probe beam at a 633-nm wavelength with $\bar{r}_{\text{eff}} = 250$ pm/V (assuming negligible difference between n_b and $\bar{n}_b$). The dashed lines now indicate the number of guided modes at $u_0 = (2)^{1/2}$, 2, 4, and 7. Obviously, in this case, the number of guided modes at any given u_0 is smaller than that for $\alpha_1 = \alpha_2 = 1$ for $u_0 > 1$, and the spacing between adjacent modes is also wider.[22] In Fig. 1, we also show the normalized profiles (dotted curves, v_2) of the corresponding highest-order guided modes, $v_2/v_{2,\max}$, for $\alpha_1\alpha_2 = 0.697$. Note that since, in this case, the guided beam is at a longer wavelength, the highest guided mode is of a lower order whenever the induced waveguide is multimode [Figs. 1(b) and 1(c)]. Also, the confinement of any guided mode is smaller than that of the same mode for $\alpha_1 = \alpha_2 = 1$ (when the soliton and guided beam are of the same wavelength).

Intuitively, the monotonic increase in the number of guided modes as a function of u_0, shown in Figs. 2 and 3, can be easily understood from waveguide theory. As shown in Ref. 14, the refractive-index change $\Delta n(x)$ is generated (via the Pockels effect) by the electric space-

charge field $\hat{E}$, with $\Delta n(x) \propto -|E_{sc}| \propto -[u^2(x) + 1]^{-1}$. At position $x = \pm d/2$, where $u^2(x = \pm d/2) = {u_0}^2/({u_0}^2 + 2)$, $\hat{E}$ and $\Delta n(x)$ attain half their maximum values. The separation between these two points, d, is the FWHM of the soliton-induced waveguide. Figure 4 illustrates the soliton-induced waveguides for two particular values of ${u_0}^2 = 4$ and ${u_0}^2 = 20$ at a given actual dimensional soliton size. As is clearly apparent from this figure, the higher the intensity ratio ${u_0}^2$, the larger is d, and the more similar is the soliton-induced index change to that of a step-index waveguide. Photorefractive screening solitons are characterized by an existence curve that relates the soliton width $\Delta\xi$ to intensity ratio ${u_0}^2$ (see Fig. 3 of Ref. 14). The variable $\Delta\xi = \Delta x k n_b (r_{\text{eff}}|V/l|)^{1/2} = (\Delta x 2\pi/\lambda)(2n_b|\Delta n_0|)^{1/2}$ is the dimensionless soliton FWHM, where Δx is the actual dimensional soliton FWHM. $\Delta\xi$ reaches a minimum roughly at intensity ratio 3. For ${u_0}^2 > 3$, one has to increase $|V/l|$ to keep Δx constant with increasing ${u_0}^2$. This increases the maximum change to the refractive index $|\Delta n_0|$, making the soliton-induced waveguide deeper (Fig. 4). The net effect of increasing ${u_0}^2$ for a fixed soliton size Δx is a both wider and deeper waveguide. This in turn implies that the induced waveguide has a larger critical guiding angle and can guide more modes as ${u_0}^2$ increases. A similar behavior was predicted for solitons in general saturable nonlinear media.[23] On the other hand, for ${u_0}^2 \ll 1$ (the low-intensity-ratio regime), Eq. (7) simplifies to

$$u'' = \left(\frac{{u_0}^2}{2} - u^2\right)u, \tag{16}$$

which has the solution $u(\xi) = u_0 \operatorname{sech}(u_0\xi/2)$, of the same form of a bright optical Kerr soliton.[14] Similar to a Kerr soliton, the bright screening soliton in this regime will induce only single-mode waveguides. In the region $0.01 \lesssim {u_0}^2 < 3$, the induced waveguide reaches its minimal width and starts to guide the second mode.

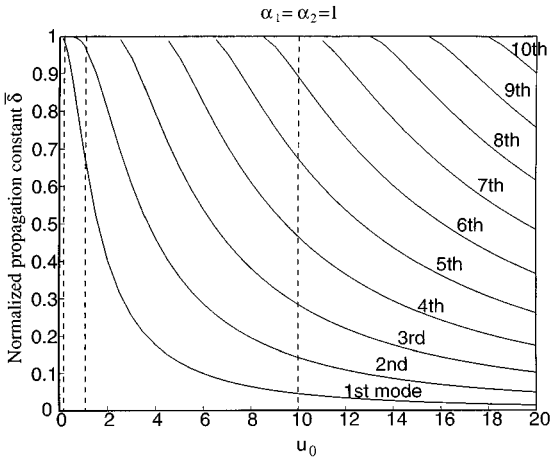

Fig. 2. Propagation constants of the guided modes of the waveguide induced by a bright screening solitons when $\alpha_1 = \alpha_2 = 1$ (same λ and polarization). The dashed lines correspond to (a) $u_0 = 0.1$, (b) $u_0 = 1$, and (c) $u_0 = 10$ of Fig. 1, at which the soliton-induced waveguides have one, two, and six guided modes, respectively.

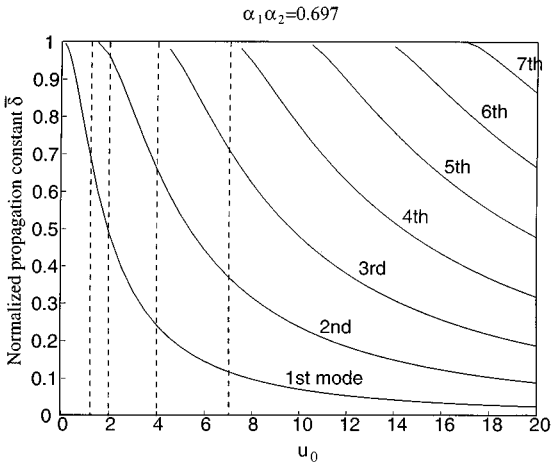

Fig. 3. Propagation constants of the guided modes of the waveguide induced by the bright screening solitons when $\alpha_1\alpha_2 = 0.697$. The dashed lines at $u_0 = (2)^{1/2}$, 2, 4, and 7 correspond to the experiments described in Section 3.

B. Waveguides Induced by Dark Solitons

To generate a dark soliton, Δn needs to be positive, as does V/l.[14] Using Eq. (8) and the normalization $E = \hat{E}/(V/l)$, we obtain the refractive index

$$\bar{n}(x) = \bar{n}_b + \Delta\bar{n}(x) = \bar{n}_b + \frac{1}{2}\bar{n}_b{}^3\bar{r}_{\text{eff}}\frac{V}{l}\frac{{u_\infty}^2 + 1}{u^2(x) + 1}. \tag{17}$$

Using the same normalized propagation constant $\bar{\delta}$ and normalization factors α_1 and α_2 as in Eqs. (13)–(15), we rewrite Eq. (9) as

$$\frac{d^2v}{d\bar{\xi}^2} = \left[\bar{\delta} - \frac{{u_\infty}^2 + 1}{u^2(\bar{\xi}/\alpha_1\alpha_2) + 1}\right]v. \tag{18}$$

When $\alpha_1 = \alpha_2 = 1$, Eq. (18) becomes

$$\frac{d^2v}{d\xi^2} = \left[\frac{\bar{\beta}^2 - k^2}{2kb} - \frac{{u_\infty}^2 + 1}{u^2(\xi) + 1}\right]v. \tag{19}$$

By comparing Eq. (19) with Eq. (7) [applied for dark solitons, i.e., $\eta = (1 + {u_\infty}^2)$, and choosing the lower sign], we know that one of the eigenfunctions (guided modes) $v(\xi)$ of Eq. (19) is identical to $u(\xi)$ of Eq. (7) with the eigenvalue $(\bar{\beta}^2 - k^2)/2kb = 1$ (or $\bar{\beta} = k + \Gamma$ since $\Gamma/k \ll 1$ and $\Gamma/b = 1$). Because the amplitude of the dark soliton, $u(\xi)$, has only one zero at $\xi = 0$ and is a constant at $\xi \to \pm\infty$, the dark soliton is indeed the second guided mode at cutoff of the waveguide induced by the dark soliton itself. This idea was first introduced in Ref. 21 and can be extended to all other nonlinear media with a local response. As a result, a waveguide induced by a one-dimensional dark soliton can support only one guided mode, as long as $\alpha_1\alpha_2 \lesssim 1$.

We now wish to find the modes of the waveguide, $v(\bar{\xi})$, in a waveguide induced by the dark soliton $u(\xi)$. We solve Eq. (18) by the shooting method after solving Eq. (7)

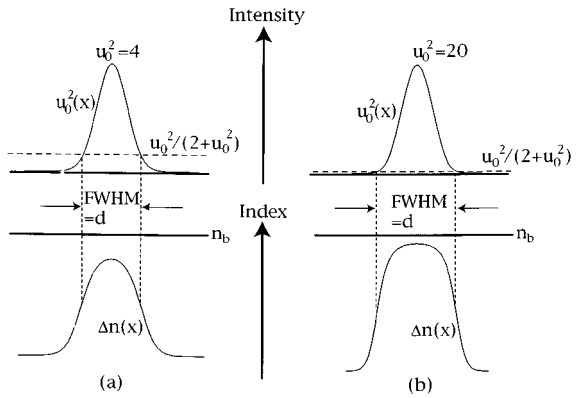

Fig. 4. Illustration of the refractive-index profiles of the waveguide induced by bright screening solitons of intensity ratios (a) 4 and (b) 20.

for the dark soliton numerically. Once again, $\bar{\delta}$ must be in the range between unity and $u_\infty{}^2 + 1$ to fulfill the condition that the propagation constant of a guided mode, $\bar{\beta}$, lies between the maximum and the minimum values of the refractive index $\bar{n}(x)$ times $\bar{k}_0$. Figure 5 shows the normalized amplitude of the dark soliton $u(\xi)/u_\infty$ (dashed curve) and the normalized amplitude of the single guided mode $v(\xi)/v(0)$ (solid curve) when $\alpha_1 = \alpha_2 = 1$ at various values of u_∞ (0.1, 1, and 10). It reveals that the higher the intensity ratio, the more confined is the optical energy near the center of the dark soliton. Figure 6 shows the propagation constant as a function of u_∞ for $\alpha_1 = \alpha_2 = 1$ and for $\alpha_1\alpha_2 = 0.734$. The latter case corresponds to a dark soliton at a 514-nm wavelength in SBN with $r_{\text{eff}} = 248$ pm/V and guiding within it a probe beam at a 632-nm wavelength with $\bar{r}_{\text{eff}} = 205$ pm/V, assuming negligible difference between n_b and $\bar{n}_b$.

From Eq. (17), it is apparent that $\Delta\bar{n}(x)$ has its maximum value $\Delta\bar{n}_0(u_\infty{}^2 + 1)$ at the center of the dark soliton, and it attains half its maximum value at position $x = \pm d/2$, where $u^2(x) = u_\infty{}^2/(u_\infty{}^2 + 2)$. The separation between these two points, d, is defined as the FWHM of the soliton-induced waveguide as shown in Fig. 7. It is apparent that the induced waveguide becomes higher and narrower as $u_\infty{}^2$ increases [Figs. 7(a) and 7(b)]. Note that, for $u_\infty{}^2 > 1$, the FWHM of the soliton remains roughly constant in accordance with Ref. 14. One can qualitatively understand from waveguide theory that the number of the guided mode should remain unchanged for various u_∞ values since the numerical aperture, $u_\infty(2n_b\Delta n_0)^{1/2}$, times the width (FWHM) of the induced waveguide is roughly kept constant (one can numerically show that rather easily).

To summarize, a waveguide induced by a dark screening soliton has a single guiding mode, of which the confined energy (confinement factor) and propagation constant are monotonically increasing with intensity ratio $u_\infty{}^2$.

3. EXPERIMENTAL RESULTS

In previous experiments, a probe beam at a less photosensitive wavelength than that used to create the soliton was guided in the waveguide induced by the bright or the dark screening solitons.[12,13,15] The idea that the number of guided modes of a waveguide induced by a two-dimensional[15] (one-dimensional[16]) bright screening soliton depends on the intensity ratio $u_0{}^2$ has also been dem-

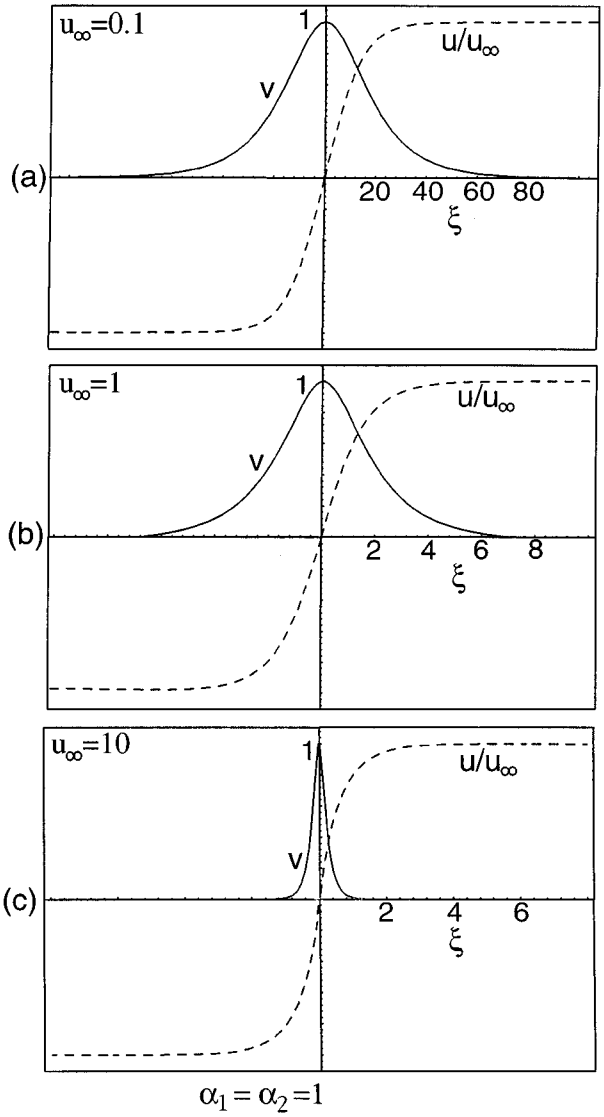

Fig. 5. Amplitude profiles of the dark screening soliton (dashed curves) and the single guided mode (solid curves) of the soliton-induced waveguide at (a) $u_\infty = 0.1$, (b) $u_\infty = 1$, and (c) $u_\infty = 10$. $u(\xi)$ is normalized to u_∞ and $v(\xi)$ to $v(0)$.

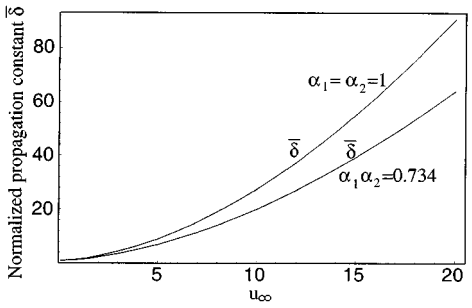

Fig. 6. Propagation constants of the guided modes of the waveguide induced by a dark screening soliton when $\alpha_1 = \alpha_2 = 1$ and $\alpha_1\alpha_2 = 0.734$.

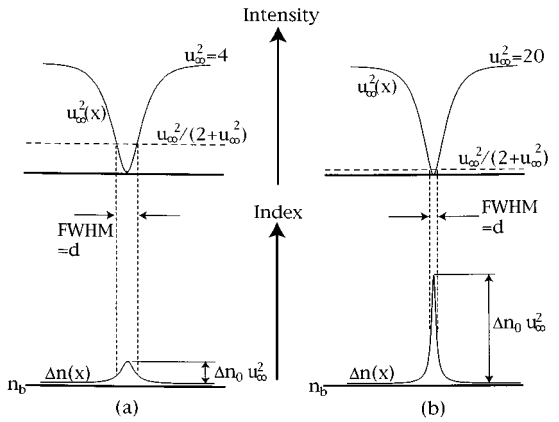

Fig. 7. Illustration of the refractive-index profiles of the waveguides induced by dark screening solitons of intensity ratios (a) 4 and (b) 20.

onstrated experimentally. In this section, we provide direct experimental proof of the modal properties of waveguides induced by one-dimensional bright and dark screening solitons, which agrees very well with the calculation above.

A. Waveguides Induced by Bright Solitons

The experimental setup is similar to that of Ref. 15, except that both the soliton and the probe beams are now one-dimensional and launched with cylindrical lenses, as shown in Fig. 8. The soliton beam is from an Ar^+ laser of a λ = 488-nm wavelength, whereas the probe beam is from a He–Ne laser with a λ=633-nm wavelength. To utilize the maximum electro-optic coefficient r_{33} of the SBN crystal (whose refractive index n_b is 2.35), both the soliton and probe beams are extraordinarily polarized. We measure the electro-optic coefficient by a separate interference experiment and find r_{eff} = 307 pm/V and r_{eff} = 250 pm/V for wavelengths λ = 488 nm and λ = 633 nm, respectively. The soliton beam has its minimum beam waist at the input face of the crystal with a width of 12 μm FWHM (widths of bright or dark solitons in the experimental section are all measured at FWHM) in the direction parallel to the crystalline c axis and nearly uniform (4 mm long) in the other transverse dimension [Fig. 9(a)]. After 4.4 mm of propagation, it diffracts roughly to 37 μm [Fig. 9(c)] with no externally applied voltage. To control the intensity ratio $u_0{}^2$,we illuminate the entire crystal with a uniform, ordinarily polarized, background beam of the same wavelength as that of the soliton. To investigate the modal properties of the soliton-induced waveguide, we launch the probe beam directly into the waveguide so that its center coincides with that of the soliton. The lowest-guided mode is directly excited by this one-dimensional fundamental Gaussian beam. To excite higher guided modes, however, we must generate zero crossings across the input probe beam, such that it will have the same number of zero crossings as the guided mode we wish to excite. We therefore insert two thin pieces of glass into the path of the He–Ne laser probe beam (before the cylindrical lens). By tilting the thin pieces (Fig. 8), we are able to generate two $(2m + 1)\pi$ phase jumps inside the probe beam to simulate the TEM_{20} mode. The minimum beam waist of the probe beam at the input face of the crystal is shown in Fig. 9(b), and the profile and photograph of the diffracted beam at the output face of the crystal is shown in Fig. 9(d).[24]

We first create a one-dimensional screening soliton [Fig. 9(e)] by applying an electric field of 3.04 kV/cm (in the polarity that generates a negative Δn_0) with intensity ratio $u_0{}^2$ = 49. Since at this intensity ratio, the fourth mode is on the edge of the cutoff frequency (Fig. 3), the third mode is thus well confined in the soliton-induced waveguide. Figure 9(f) shows the photograph and the profile of the guided third mode at the output face of the crystal. We then reduce the intensity ratio $u_0{}^2$ to 16 and the electric field to 2.36 kV/cm accordingly[11,14] to keep the same FWHM of the soliton [Fig. 9(g)]. The third mode cannot be guided effectively [Fig. 9(h)], although some guiding effect is observed [as compared to Fig. 9(d)] because at intensity ratio $u_0{}^2$ = 16, the third mode is just on the edge of cutoff (Fig. 3). Finally, we reduce the intensity ratio $u_0{}^2$ to 4 and adjust the voltage to 1650 V/cm accordingly, where the third mode does not exist. The beam of Fig. 9(j) ($u_0{}^2$ = 4) is clearly less confined than that of Fig. 9(h) ($u_0{}^2$ = 16). However, because the inner product between the TEM_{20} mode and the first (fundamental) guided mode of the soliton-induced waveguide is nonzero, the central lobe in Fig. 9(j) is efficiently confined by the soliton-induced waveguide, whereas the sidelobes are scattered away by the waveguide.

We repeat the same procedure for the TEM_{10} mode, for which we insert only one thin piece of glass into the center of the probe He–Ne laser beam. Figure 10(a) shows the photograph and profile of the beam at the input face of the crystal. The experimental results, Figs. 10(b)–10(e), agree well with the number of modes given by the number of intersections of dashed vertical lines in Fig. 3 at various intensity ratios. At intensity ratios 49 and 16 [Figs. 10(b) and 10(c)], the second mode is well confined in the induced waveguide, whereas at intensity ratios 4 and 2 (the second mode is at the vicinity of cutoff, Fig. 3) the second mode cannot be guided effectively [Figs. 10(d) and 10(e)]. Finally, we remove the thin piece of glass and let the probe beam be TEM_{00} mode. The experimental results are shown in Fig. 11. At intensity ratio 2, the probe beam is well confined [Fig. 11(c)] since the fundamental mode always exists for all intensity ratios. This confirms the theoretical results presented in Fig. 3, which shows that the number of guided modes in a waveguide induced by a photorefractive bright screening soliton is a monotonically increasing function of the intensity ratio.

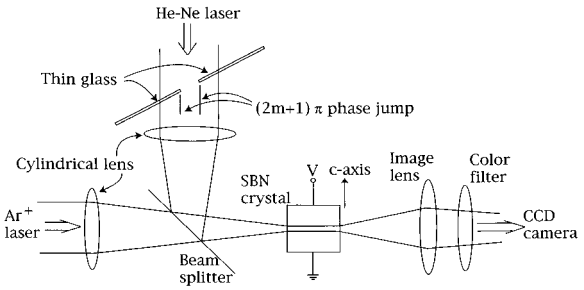

Fig. 8. Experimental setup for investigating waveguides induced by bright screening solitons.

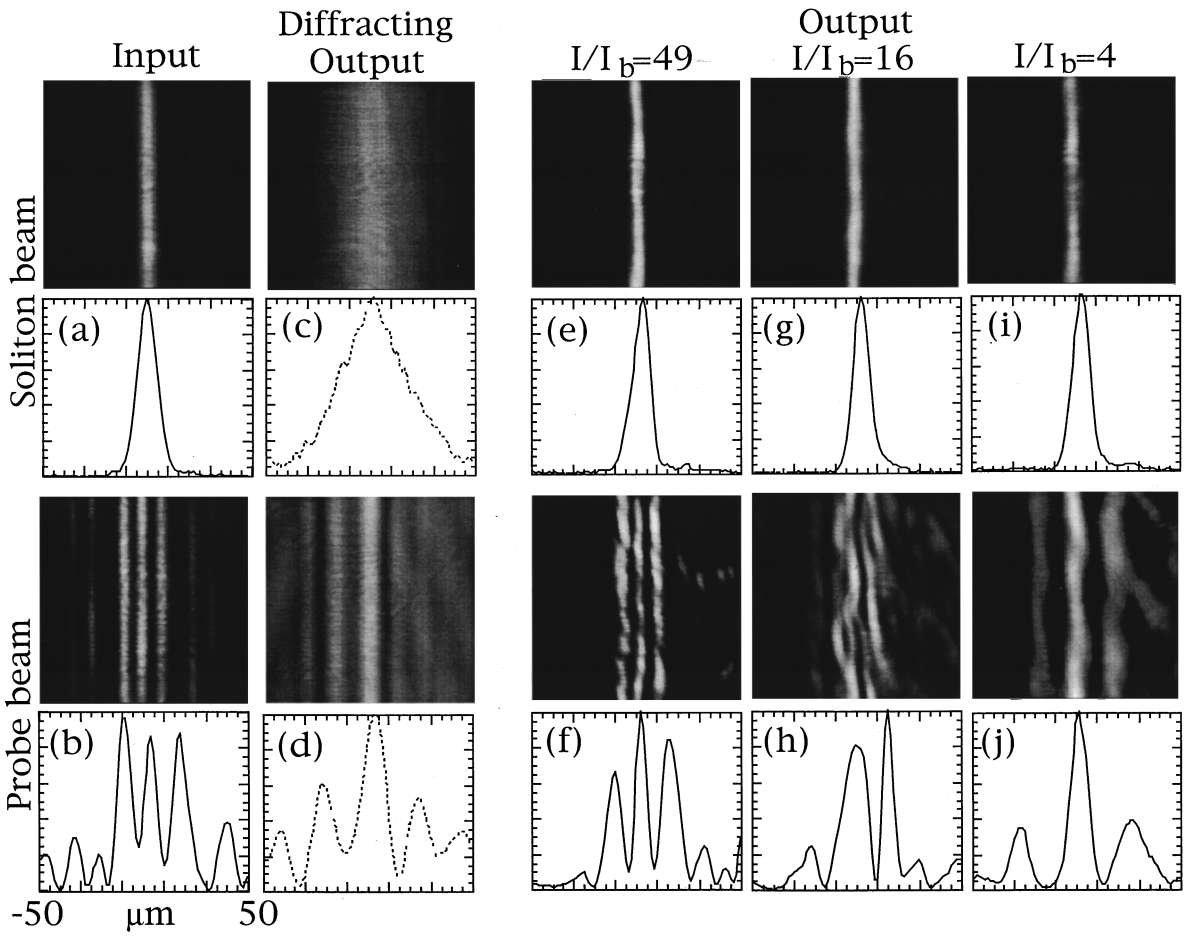

Fig. 9. Photographs and beam profiles of [(a), (c)] the 488-nm laser beam and [(b), (d)] the probe beam of TEM_{20} mode at the input and exit faces of the unbiased crystal. Photographs and beam profiles of the soliton beam and the probe beam at the exit face of the crystal are at intensity ratios ${u_0}^2$ equal to (e), (f) 49; (g), (h) 16; and (i), (j) 4.

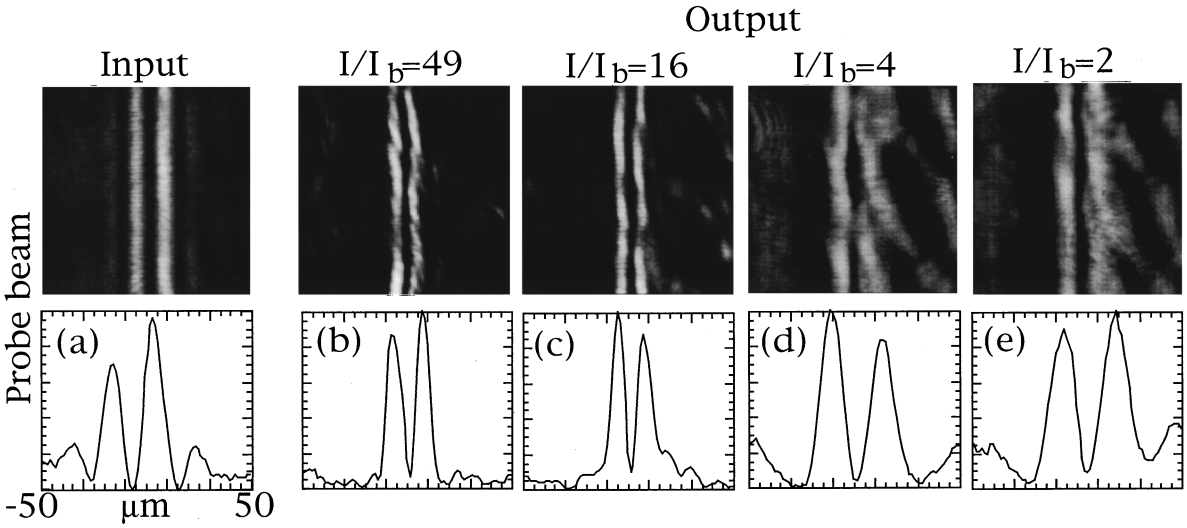

Fig. 10. Photographs and beam profiles of a probe beam of TEM_{10} mode at (a) the input face and at (b)–(e) the exit face of the crystal at intensity ratios ${u_0}^2$ equal to (b) 49, (c) 16, (d) 4, and (e) 2.

B. Waveguides Induced by Dark Solitons

The experimental setup to probe the waveguide induced by dark solitons is the same as that in Ref. 12. The soliton beam is from an Ar^+ laser at a 514-nm wavelength, and the probe beam is from a He–Ne laser with a 633-nm wavelength. A different SBN crystal is used for the experiment of the dark-soliton-induced waveguides, which was grown by the vertical Bridgman method. The refractive index n_b is now 2.35 and the electro-optic coefficient r_{33} is 280 pm/V (270 pm/V) for the soliton beam (probe

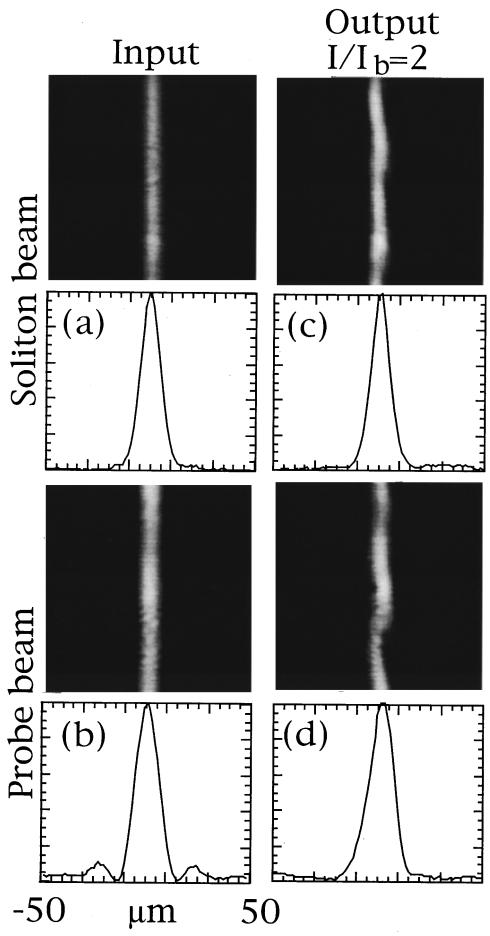

Fig. 11. Photographs and beam profiles of [(a), (c)] the soliton beam and [(b), (d)] the probe beam of TEM_{00} mode at the input and exit faces of the crystal.

beam). This gives rise to a normalization factor product $\alpha_1\alpha_2$ equal to 0.8, for which the propagation constant of the probe beam lies between the two curves in Fig. 6, still experiencing a single-mode waveguide. The dark soliton beam is extraordinarily polarized, collimated large enough to cover the entire crystal uniformly, and reflected from a $\lambda/4$ step mirror to bear a π-phase jump in the center of the beam (the origin of the dark soliton). An ordinarily polarized, uniform, background illumination is launched to cover the entire crystal for controlling the intensity ratio. The dark notch at the input face of the crystal is 19 μm wide [Fig. 12(a)]. It diffracts to 35 μm at the output face [Fig. 12(d)] of the crystal after 11.7 mm of propagation. The fundamental mode of the probe beam diffracts from 16 μm [Fig. 12(b)] to 90 μm [Fig. 12(e)] within the same propagation distance.

Without background illumination, which implies that the intensity ratio approaches infinity, we apply -180 V between the electrodes, which are separated by 5.3 mm. After the dark soliton forms, as shown in Fig. 12(g), taken at the exit face of the crystal, the probe beam in the fundamental mode is confined to 23 μm within the soliton-induced waveguide [Fig. 12(h)]. We then insert a thin piece of glass into the probe beam and tilt the glass to generate a $(2m + 1)\pi$-phase jump at the center of the probe beam so as to simulate the TEM_{10} mode [Fig. 12(c)]. In the absence of the soliton-induced waveguide, this beam diffracts [Fig. 12(f)]. As expected from the above prediction that dark solitons induce only single-mode waveguides when $\alpha_1\alpha_2 < 1$, the second mode does not exist at any intensity ratio. Therefore no waveguiding effect is observed for the second-mode beam [Fig. 12(i)] under this condition. We then reduce the intensity ratio to 2 by adding background illumination, increase the voltage to -320 V accordingly,[12,14] and generate the dark soliton shown in Fig. 12(j). Repeating the above procedure with the first and second modes of the probe beam, we find that at this intensity ratio the soliton-induced waveguide is single-mode [Figs. 12(k) and 12(l)]. We test this at another intensity ratio (of 5) and find the same result. This confirms that waveguides induced by photorefractive dark screening solitons are single mode, as predicted by the theory in the previous section, as long as $\alpha_1\alpha_2 < 1$.

4. DISCUSSION

In the theoretical section of this paper, two assumptions were made: (1) The polarization of the probe beam is parallel to one of the principal crystalline axes, and (2) the intensity of the probe beam does not affect the soliton-induced waveguide. The first assumption does not restrict the theoretical treatment even when the polarization of the probe beams is not parallel to the principal crystalline axes. Furthermore, one can straightforwardly generalize the theory for an arbitrarily polarized probe beam by decomposing it into two eigenpolarization components, with each parallel to a principal axis. This problem is then simplified to solving for a probe beam propagating in a birefringent waveguide. Notice that this equivalent birefringent waveguide can have different index depths for both polarizations, yet the widths are identical. This is because the depth of the waveguide depends on the electro-optic coefficient r_{eff}, whereas its width depends only on the intensity distribution of the soliton, $u^2(x)$, irrespective of the guided (probe) beam. The second assumption can be more restrictive but does not cause any problem in photorefractive media as long as the absorption of the probe beam is much smaller than that of the soliton. On the other hand, if the probe beam is of a photosensitive wavelength that excites the electrons from midgap donors to the conduction band, it will affect the soliton. The problem can be treated in a manner similar to that of coupled soliton pairs, which has been thoroughly studied recently.[25–27]

5. APPLICATIONS

The use of solitons, in particular photorefractive solitons, to induce waveguides in a bulk medium brings about several interesting applications. Some potential applications are common to all spatial solitons in Kerr and non-Kerr nonlinear media. These include reconfigurable near-field optical interconnects and optical wiring. For these applications, the only advantage photorefractive

solitons have over Kerr solitons[28] is the dimensionality: Since photorefractive solitons can self trap in both transverse dimensions,[2,7,17,18] they can induce two-dimensional waveguides.[15] But the recently discovered quadratic solitons[29] and solitons in saturable nonlinear media[30] were shown to exhibit two-dimensional self-trapping and are expected to induce two-dimensional waveguides as well. There are, of course, several major differences in the properties of the soliton-induced waveguides in each of these cases (such as optical power required, response time, and energy required for switching), which have been discussed at length in Ref. 14. On this subject we just add two recent advances with photorefractive solitons. The first is a recent observation of self-trapping in photorefractive semiconductors (InP) and induced waveguiding, which was carried out at an optical telecommunication wavelength (1.3 μm) and with a formation time of the order of microseconds.[31,32] The second is the creation of very fast high-intensity screening solitons, which was predicted in Ref. 14 and recently observed in SBN with a pulsed laser at nanosecond time scales.[33]

A second application of photorefractive solitons utilizes soliton-induced waveguiding for beam steering. This application is commonly referred to as soliton dragging, in which an intense soliton beam is able to guide and steer a weak signal beam, and which was observed in Kerr[34] and quadratic media.[35] What makes photorefractive solitons unique for beam-steering applications is their wavelength sensitivity. When the photorefractive solitons are created at a highly sensitive wavelength, and the signal (probe) beam is at a nonphotosensitive wavelength, a very weak (microwatt) soliton beam can guide and steer an intense probe beam. This idea was demonstrated with photorefractive quasi-steady-state solitons,[13] screening solitons,[12,15] and photovoltaic solitons.[4]

The last and most unique application of waveguides induced by photorefractive solitons is for nonlinear frequency conversion, which was first proposed in Ref. 14. Since the conversion efficiency of second-harmonic generation and other $\chi^{(2)}$ parametric processes always scales with the optical intensity of the pump beam, it is desirable to confine the interacting beams in a waveguide

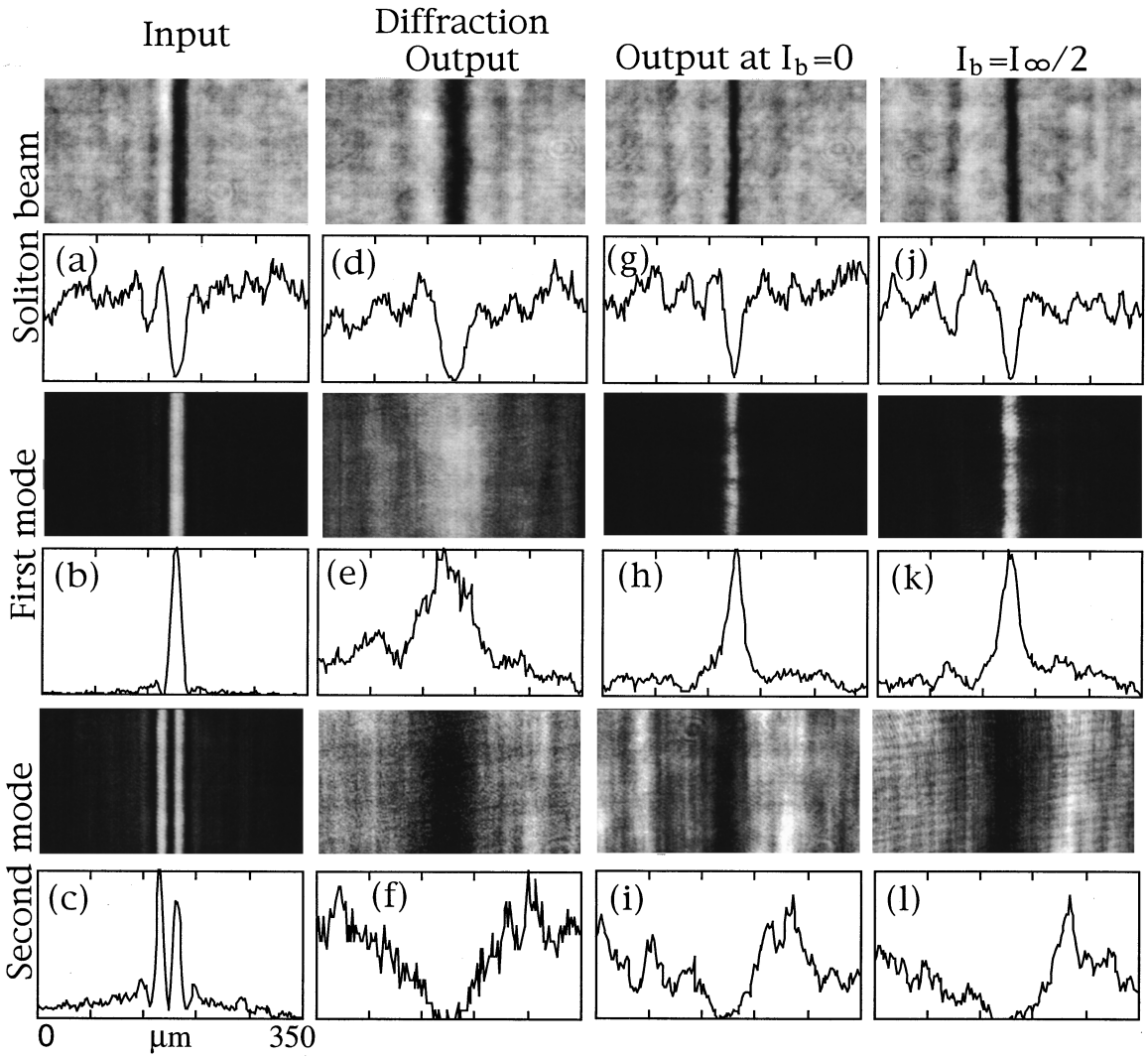

Fig. 12. Photographs and beam profiles at [(a)–(c)] the input and [(d)–(l)] the exit faces of the crystal for the dark soliton beam and of probe beams of TEM_{00} and TEM_{10} modes. Since the diffraction pattern in the x direction is too large to fit into our CCD camera under the same magnification as the other photographs, we show here only the truncated photographs and profiles in (f), (i), and (l).

structure. This implies that phase matching is now required among the propagation constants of the interacting guided modes of the waveguide (rather than among the wave vectors, as in a bulk medium). Phase matching can be obtained by use of either birefringence or periodic poling (quasi-phase matching). With a fabricated waveguide, there is very little second-harmonic-generation wavelength tuning possibility[36] with either phase-matching technique because the structure is fixed (parametric amplifiers, of course, allow more tunability because one has the freedom of varying both pump and idler). Typical tuning techniques include angle and temperature tuning (see Ref. 36 for a detailed discussion). Since both have a very limited tunability range for second-harmonic generation in waveguides, structures with several (laterally parallel to each other) periods of poling were fabricated,[37] giving rise to extended tuning. Obviously, it is highly desirable to have waveguide structures in which either the phase matching (periodic poling or crystalline directions) or the waveguide properties (propagation constants) are tunable without mechanical movements.

Waveguides induced by photorefractive solitons offer just that: a large degree of tuning of all the waveguide parameters. Since most photorefractive materials are noncentrosymmetric crystalline media, they exhibit large second-order nonlinearities. Thus nonlinear frequency conversion can be efficiently done in waveguides induced by photorefractive solitons. Several features of photorefractive solitons make this possible and very attractive. First, the waveguides can be induced by very weak soliton beams, and two (or three) intense beams can be guided in them, all of longer wavelengths, interacting with each other via $\chi^{(2)}$. A second alternative would include configurations in which the shorter-wavelength beam (which is generated in the frequency-conversion process) also forms a soliton, which, at the same time, confines (guides) the other (pump, idler) beams as well. Third, phase matching at a specific operation point can be achieved by use of crystalline birefringence (such as in photorefractive $KNbO_3$) or by periodic poling. The latter can be done by means of standard electrical poling techniques[36,37] as in $LiNbO_3$ and SBN (Ref. 38) or by more exotic means, which utilize photorefractive space-charge fields as demonstrated in $BaTiO_3$ (Ref. 39), SBN (Refs. 40–42), and $KNbO_3$ (Ref. 43). Especially notable is the result reported in Ref. 38, which has shown high efficiency of periodic poling and of second-harmonic generation in the very same crystal we use in the present paper for generating solitons: SBN. Finally, as shown in the present paper, waveguides induced by screening solitons are highly controllable by electro-optic means (no mechanical movements needed), simply by tuning the soliton along its existence curve. As shown in Figs. 2, 3, and 6, the propagation constants of the fundamental guided mode are tunable, by a factor $|\Delta n_0|/n_b$ for bright solitons and by $\sim 100(|\Delta n_0|/n_b)$ for dark solitons, by simply varying the soliton-intensity ratio and applied voltage to walk along the existence curve. This means that the phase-matching condition, whether it is achieved by birefringence or by periodic poling, is highly tunable (especially for waveguides induced by dark solitons), with a very large degree of accuracy. We foresee that the combination of flexible phase matching and high-power confinement in waveguides induced by photorefractive solitons will lead to efficient and highly tunable nonlinear frequency converters.

6. CONCLUSIONS

In this paper, we have shown that the modal properties of the waveguides induced by the bright and dark one-dimensional screening solitons depend on the ratio between the peak intensity of the soliton and the sum of the background illumination and the dark irradiance. The number of guided modes in a waveguide induced by a bright soliton increases monotonically with increasing intensity ratio, whereas waveguides induced by dark solitons are always single mode for all intensity ratios. In both cases, the wavelength of the probe beam is assumed to be longer than that of the soliton, for which the photorefractive crystal is less photosensitive. The propagation constants of the guided modes are a function of the intensity ratio and can be tuned continuously for both bright- and dark-soliton-induced waveguides. Our experimental results show very good agreement with the theoretical calculations. Finally, we discuss several applications utilizing waveguides induced by the photorefractive screening solitons.

ACKNOWLEDGMENTS

M. Segev gratefully acknowledges the support of the Sloan Foundation. This research is supported by the U.S. Army Research Office and the National Science Foundation.

*Also with the Department of Materials Science and Engineering, Stanford University, Stanford, California 94305.

†Also with 3D Technology Labs, 210 Kittoe Drive, Unit B, Mountain View, California 94043.

REFERENCES AND NOTES

1. M. Segev, B. Crosignani, A. Yariv, and B. Fischer, Phys. Rev. Lett. **68**, 923 (1992).
2. G. Duree, J. L. Shultz, G. Salamo, M. Segev, A. Yariv, B. Crosignani, P. DiPorto, E. Sharp, and R. Neurgaonkar, Phys. Rev. Lett. **71**, 533 (1993).
3. G. C. Valley, M. Segev, B. Crosignani, A. Yariv, M. M. Fejer, and M. Bashaw, Phys. Rev. A **50**, R4457 (1994).
4. M. Taya, M. Bashaw, M. M. Fejer, M. Segev, and G. C. Valley, Phys. Rev. A **52**, 3095 (1995).
5. M. Segev, G. C. Valley, B. Crosignani, P. DiPorto, and A. Yariv, Phys. Rev. Lett. **73**, 3211 (1994).
6. Steady-state self-focusing effects in biased photorefractive media were first observed by M. D. Iturbe-Castillo, P. A. Marquez-Aguilar, J. J. Sanchez-Mondragon, S. Stepanov, and V. Vysloukh, Appl. Phys. Lett. **64**, 408 (1994).
7. Screening solitons were first observed by M. Shih, M. Segev, G. C. Valley, G. Salamo, B. Crosignani, and P. DiPorto, Electron. Lett. **31**, 826 (1995); Opt. Lett. **21**, 324 (1996).
8. D. N. Christodoulides and M. I. Carvalho, J. Opt. Soc. Am. B **12**, 1628 (1995).
9. G. Duree, J. L. Shultz, G. Salamo, M. Segev, A. Yariv, B. Crosignani, P. DiPorto, E. Sharp, and R. Neurgaonkar, Phys. Rev. Lett. **74**, 1978 (1995).

10. Z. Chen, M. Segev, D. W. Wilson, R. E. Muller, and P. D. Maker, Phys. Rev. Lett. **78**, 2948 (1997).
11. K. Kos, H. Meng, G. Salamo, M. Shih, and M. Segev, Phys. Rev. E **53**, R4330 (1996).
12. Z. Chen, M. Mitchell, M. Shih, M. Segev, M. Garrett, and G. C. Valley, Opt. Lett. **21**, 629 (1996); Z. Chen, M. Shih, M. Segev, D. W. Wilson, R. E. Muller, and P. D. Maker, "Steady-state vortex-screening solitons formed in biased photorefractive media," Opt. Lett. (to be published).
13. M. Morin, G. Duree, G. Salamo, and M. Segev, Opt. Lett. **20**, 2066 (1995).
14. M. Segev, M. Shih, and G. C. Valley, J. Opt. Soc. Am. B **13**, 706 (1996).
15. M. Shih, M. Segev, and G. Salamo, Opt. Lett. **21**, 931 (1996).
16. M. Shih, Z. Chen, M. Segev, T. H. Coskun, and D. N. Christodoulides, Appl. Phys. Lett. **69**, 4151 (1996).
17. M. Shih and M. Segev, Opt. Lett. **21**, 1538 (1996).
18. M. Shih, M. Segev, and G. Salamo, Phys. Rev. Lett. **78**, 2551 (1997).
19. H. Meng, G. Salamo, M. Shih, and M. Segev, Opt. Lett. **22**, 448 (1997).
20. A. W. Snyder, D. J. Mitchell, and Y. S. Kivshar, Mod. Phys. Lett. B **9**, 1479 (1995).
21. A. W. Snyder, D. J. Mitchell, and B. Luther-Davies, J. Opt. Soc. Am. B **10**, 2341 (1993).
22. This statement is true whenever $\alpha_1\alpha_2 < 1$. However, several photorefractive crystals have increased sensitivity at larger wavelengths, so in principle one can generate a soliton and guide in it a probe beam of a less photosensitive but shorter wavelength, i.e., $\alpha_1 > 1$. This, of course, will increase the number of guided modes and will increase their confinement at the probe-beam wavelength.
23. A. W. Snyder, D. J. Mitchell, L. Poladian, and F. Landouceur, Opt. Lett. **16**, 21 (1991).
24. We note that, because our input beam is not an ideal TEM_{20} Gaussian beam [i.e., the horizontal beam profile shown in Fig. 9(b) is not ideally proportional to an $m = 2$ Gauss–Hermite beam], its far-field diffraction pattern [Fig. 9(d)] is not an ideal three-lobe pattern but rather has some additional structure. Nevertheless, this method enables us to excite the third guided mode in a waveguide rather efficiently because most of the optical power is at the vicinity of the three central lobes that are formed by two π-phase jumps.
25. Z. Chen, M. Segev, T. H. Coskun, and D. N. Christodoulides, Opt. Lett. **21**, 1436 (1996).
26. Z. Chen, M. Segev, T. H. Coskun, D. N. Christodoulides, Y. S. Kivshar, and V. V. Afanasjev, Opt. Lett. **21**, 1821 (1996).
27. Z. Chen, M. Segev, T. H. Coskun, D. N. Christodoulides, and Y. S. Kivshar, "Coupled photorefractive soliton pair," J. Opt. Soc. Am. B **14**, 3066–3077 (1997).
28. J. S. Aitchison, A. M. Weiner, Y. Silberberg, M. K. Oliver, J. L. Jackel, D. E. Leaird, E. M. Vogel, and P. W. Smith, Opt. Lett. **15**, 471 (1990).
29. W. E. Torruellas, A. Wang, D. J. Hagan, E. W. Van Stryland, G. I. Stegeman, L. Torner, and C. R. Menyuk, Phys. Rev. Lett. **74**, 5036 (1995).
30. V. Tikhonenko, J. Christou, and B. Luther-Davies, Phys. Rev. Lett. **76**, 2698 (1996).
31. M. Chauvet, S. A. Hawkins, G. Salamo, M. Segev, D. F. Bliss, and G. Bryant, Opt. Lett. **21**, 1333 (1996).
32. M. Chauvet, S. A. Hawkins, G. Salamo, M. Segev, D. F. Bliss, and G. Bryant, "Photo-induced two-dimensional waveguides in InP:Fe using the photorefractive effect at 1.3 mm," Appl. Phys. Lett. (to be published).
33. G. Salamo and M. Segev, Department of Physics, University of Arkansas, Fayetteville, Ark. 72701, and Department of Electrical Engineering and Center for Photonics and Optoelectronic Materials, Princeton University, Princeton, N.J. 08544, respectively (personal communication, 1997).
34. J. U. Kang, G. I. Stegeman, and J. S. Aitchison, Opt. Lett. **21**, 189 (1996).
35. W. E. Torruellas, Z. Wang, L. Torner, and G. I. Stegeman, Opt. Lett. **20**, 1949 (1995).
36. M. M. Fejer, G. A. Magel, D. H. Jundt, and R. L. Byer, IEEE J. Quantum Electron. **28**, 2631 (1992).
37. L. E. Myres, R. C. Eckardt, M. M. Fejer, R. L. Byer, and W. R. Bosenberg, Opt. Lett. **21**, 591 (1996).
38. Y. Y. Zhu, J. S. Fu, R. F. Xiao, and G. K. L. Wong, Appl. Phys. Lett. **70**, 1793 (1997).
39. F. Micheron and G. Bismuth, Appl. Phys. Lett. **20**, 79 (1972).
40. F. Micheron and G. Bismuth, Appl. Phys. Lett. **23**, 71 (1973).
41. M. Horowitz, A. Bekker, and B. Fischer, Appl. Phys. Lett. **62**, 2619 (1993).
42. A. S. Kewitsch, M. Segev, A. Yariv, G. Salamo, T. W. Towe, E. J. Sharp, and R. Neurgaonkar, Appl. Phys. Lett. **64**, 3068 (1994).
43. R. S. Cudney, P. Bernasconi, M. Zgonik, J. Fousek, and P. Gunter, Appl. Phys. Lett. **70**, 1339 (1997).